

# Syntheses, Characterizations, Luminescence Properties, and Electronic Structures of Gold(I) Bis(phosphine)–Xanthate Complexes

Zerihun Assefa, Richard J. Staples, and John P. Fackler, Jr.\*

Laboratory of Molecular and Structural Bonding, Department of Chemistry Texas A&M University, College Station, Texas 77843-3255

Received June 25, 1993\*

Syntheses, structures and photophysical properties of some bis(phosphine) xanthate complexes,  $L_2AuS_2COR$ ,  $L = Ph_3P$ , CEP(tris(cyanoethyl)phosphine) are described. Extended Hückel and Fenske–Hall molecular orbital (MO) calculations indicate that bending activates the gold(I) center for interaction with nucleophiles. Experimentally, it is observed that the compound with the smaller P–Au–P angle ( $Ph_3P$ ) also shows the shortest Au–S distance. In fact, the  $(CEP)_2AuS_2COEt$  complex has two nearly identical Au–S distances at 2.745(2) and 2.934(2) Å, which are 0.2 Å longer than the short Au–S distance, 2.530(2) Å, in the  $(Ph_3P)_2AuS_2COEt$  complex. The absorption spectra of the complexes show a moderately intense band around 306 nm ( $\epsilon = (1.5–3.0) \times 10^4 M^{-1} cm^{-1}$ ) and a weak band at ca. 390 nm ( $\epsilon = 100 M^{-1} cm^{-1}$ ). The perturbation of the  $KS_2COR$  “free” ligand anion absorption bands in  $CH_3CN$  shifts the high-energy band slightly to the blue while the low-energy band significantly blue shifts. Spectral changes observed by the systematic variation of the R groups on the xanthate and by solvent variation studies suggest that the high energy band is a  $\pi-\pi^*$  transition localized on the xanthate ligand. Each complex luminesces as a solid and in solution. Lifetimes for the solids are nanosecond in duration. Excitation spectra resemble absorption spectra. It is believed that the luminescence in these mononuclear gold(I) complexes originates from ligand excitation centered in the  $n-\pi^*$  transition. Complex 2,  $(CEP)_2AuS_2COEt$ , crystallizes in the monoclinic space group  $P2_1/c$  (No. 14), with  $a = 11.538(2)$  Å,  $b = 20.302(4)$  Å,  $c = 11.565(1)$  Å,  $\beta = 116.62(1)^\circ$ ,  $Z = 4$ , and  $R = 0.0325$ . Compound 4,  $(Ph_3P)_2AuS_2COEt$ , crystallizes in the triclinic space group  $P\bar{1}$  (No. 2), with  $a = 10.316(3)$  Å,  $b = 13.058(2)$  Å,  $c = 14.039(4)$  Å,  $\alpha = 88.07^\circ$ ,  $\beta = 74.40^\circ$ ,  $\gamma = 76.59(1)^\circ$ ,  $Z = 2$ , and  $R = 0.0273$ .

## Introduction

Depending<sup>1</sup> upon the electronic and steric features of the tertiary phosphine, and concentrations used in synthesis, two-, three-, and four-coordinate gold(I) phosphine complexes form.<sup>2–8</sup> Substituents on the phosphorus in the bis(phosphine)–Au(I) complexes also influence the ability of additional ligands to coordinate to the metal atom.<sup>2</sup> With monodentate arylphosphines such as  $Ph_3P$ , anions such as  $Cl^-$  or  $SCN^-$  readily coordinate, forming three-coordinate  $AuL_2X$  species. Coordination of  $SCN^-$ , however, to  $[(cyclo-C_6H_{11})_3P]_2Au^+$  is very weak<sup>4</sup> and the P–Au–P angle remains close ( $177.4^\circ$ ) to  $180^\circ$ .

The coordinating ability of the non-phosphine ligand also is of importance. With the bidentate nitrogen ligand bipyridine, a

distorted three-coordinate species is obtained<sup>6</sup> upon bonding to  $[Ph_3PAu]^+$ , but with dithiocarbamate ligands<sup>7</sup> a nearly linear P–Au–S ( $175.7^\circ$ ) coordination results. Chelation is not observed in the crystalline material<sup>4</sup> (although the complex is probably fluxional in solution). With 1,2-dicyano-1,2-dithiol the Au(I) center also shows 3-coordination.<sup>9</sup>

Theoretical studies of  $PtL_2$ , with  $d^{10}$  valence electron structures, show almost no Pt  $5d_{z^2}$  orbital involvement in the P→M  $\sigma$ -bonding. Goddard<sup>10</sup> and Morokuma<sup>11</sup> have analyzed the effect that changes in the P–Pt–P angle have upon oxidative addition. Bending the P–Pt–P angle efficiently and selectively raises the energy of one of the d orbitals ( $d_{yz}$ ) thereby promoting electron transfer to the incoming ligand as the ligand coordinates to the metal. Similar results are to be expected with the  $d^{10} L_2Au^+$  complexes.

Here we describe syntheses, structural characterizations and spectroscopic properties of some xanthate complexes of bis-(phosphine)gold(I) cations. Ligand and solvent variations have provided a basis for analysis of the absorption and emission spectra. Relativistically parametrized extended Hückel calculations<sup>12</sup> have been performed on energy-minimized structures obtained using the MM2 program of the CAChe system. The various results are compared.

## Experimental Section

The compounds  $CEP_2AuCl$  and  $(Ph_3P)_2AuCl$  were synthesized following literature methods.<sup>2,13</sup> All reactions were carried out in an atmosphere of prepurified  $N_2$ . Solvents used were rigorously dried and

\* Author to whom correspondence should be addressed.

• Abstract published in *Advance ACS Abstracts*, May 15, 1994.

- (1) Abbreviations used in this paper: CEP, tris(cyanoethyl)phosphine;  $PPh_3$ , triphenylphosphine; L,  $PPh_3$ , CEP; AN, acetonitrile, Me,  $CH_3$ ; Et,  $CH_2CH_3$ ; Bu,  $CH_2CH_2CH_2CH_3$ ; HE, high energy; LE, low energy; EH, extended Hückel; HOMO, highest occupied molecular orbital; LUMO, lowest unoccupied molecular orbital; SHOMO, second highest occupied molecular orbital; PL, photoluminescence; LMCT, ligand to metal charge transfer; UV, ultraviolet.
- (2) Bensch, W.; Prelati, M.; Ludwig, W. *J. Chem. Soc., Chem. Commun.* **1986**, 1762. Mann, B. E.; Musco, A. *J. Chem. Soc., Dalton Trans.* **1980**, 776. Baenziger, N. C.; Dittmore, K. M.; Doyle, J. R. *Inorg. Chem.* **1974**, *13*, 805.
- (3) Muir, J. A.; Muir, M. M.; Arias, S., *Acta Crystallogr.* **1982**, *B38*, 1318. Muir, J. A.; Muir, M. M.; Arias, S.; Campana, C. F.; Dwight, S. K., *Acta Crystallogr.* **1981**, *A37*, C227.
- (4) Muir, J. A.; Muir, M. M.; Lorca, E., *Acta Crystallogr.* **1980**, *B36*, 931. Guggenberger, L. J., *J. Organomet. Chem.* **1974**, *81*, 271.
- (5) CAChe (Computer Aided Chemistry), CAChe Scientific, Inc., TEKTRONIX Company, Beaverton, OR 97077.
- (6) Clegg, W. *Acta Crystallogr.* **1976**, *B32*, 2712.
- (7) Wijnhoven, J. G.; Bosman, W. P. J. H.; Beursbeur, P. T. *J. Cryst. Mol. Struct.* **1972**, *2*, 7.
- (8) Bates, P. A.; Waters, J. M. *Inorg. Chem. Acta* **1984**, *81*, 151. Khan, Md, N. I.; King, C.; Heinrich, D. D.; Fackler, J. P., Jr.; Porter, L. C. *Inorg. Chem.* **1989**, *28*, 2150. Shain, J.; Fackler, J. P., Jr. *Inorg. Chem. Acta* **1987**, *131*, 157. Jones, P. G., *J. Chem. Soc., Chem. Commun.* **1980**, 2031. Elder, R. C.; Kelle-Zeher, E. H.; Onady, M.; Whittle, R. R. *J. Chem. Soc., Chem. Commun.* **1981**, 900.

- (9) Dávila, R.; Elduque, A.; Grant, T.; Staples, R. J.; Fackler, J. P., Jr. *Inorg. Chem.* **1993**, *32*, 1749.
- (10) Low, J. J.; Goddard, W. A. *J. Am. Chem. Soc.* **1984**, *106*, 6928.
- (11) Obara, S.; Kitaura, K.; Morokuma, K. *J. Am. Chem. Soc.* **1984**, *106*, 7482.
- (12) (a) Pyykkö, P. *Chem. Rev.* **1988**, *88*, 563. (b) *Methods In Computational Chemistry*; Wilson, S., Ed.; Plenum Press: New York, 1988; Vol. 2, pp 137–221. (c) Pyykkö, P.; Lohr, L. L. *Inorg. Chem.* **1981**, *20*, 1950. (d) Mehrotra, P.; Hoffmann, R. *Inorg. Chem.* **1978**, *17*, 2187. (e) Jiang, Y.; Alvarez, S.; Hoffmann, R. *Inorg. Chem.* **1985**, *24*, 749. (f) Pyykkö, P.; Desclaux, J. P. *Acc. Chem. Res.* **1979**, *12*, 276.
- (13) Khan, M. N. I.; King, C.; Fackler, J. P., Jr.; Winpenny, R. E. *P. Inorg. Chem.* **1993**, *32*, 2502.

distilled prior to use. IR spectra were recorded on a Perkin-Elmer 783 infrared spectrometer. UV-visible studies were carried out on a Cary 17 spectrophotometer. Emission and excitation spectra, obtained with a Perkins LS2 and a Aminco-Bowman AD2 luminescence spectrofluorometer, were corrected for instrumental response. Lifetime measurements were made using ~0.8-ns excitation from the 355-nm third harmonic of a Quantel YG-481 laser.<sup>14</sup>

**Synthesis of Potassium Methyl Xanthate,  $\text{KS}_2\text{COCH}_3$ .** Pulverized KOH, 2.8 g (0.05 mol), was dissolved in 100 mL of dry MeOH. The solution was stirred for about 1/2 h. After this solution was cooled to room temperature in ice bath, 3.8 mL of  $\text{CS}_2$  (0.05 mol) was added dropwise over a period of 30 min. The solution turned yellow in a few minutes. The mixture was stirred for an hour and diethyl ether was added until a precipitate appeared permanently. After a few minutes a bulk of gelatinous light yellow precipitate appeared, which was vacuum filtered and washed with diethyl ether and dried in a desiccator containing KOH pellets.

**Synthesis of Potassium Ethyl Xanthate,  $\text{KS}_2\text{COCH}_2\text{CH}_3$ .** Pulverized KOH 2.8 (0.05 mol) was dissolved in 100 mL of dry EtOH. The solution was stirred for about 1/2 h. After the solution was cooled to room temperature in ice bath, 3.8 mL of  $\text{CS}_2$  (0.05 mol) was added dropwise over a period of 30 min. The solution turned yellow upon  $\text{CS}_2$  addition. The mixture was stirred for an hour, and diethyl ether was added until a precipitate appeared permanently. After a few minutes a bulk of gelatinous yellowish precipitate appeared, which was vacuum filtered and washed with diethyl ether and dried in a desiccator containing KOH pellets.

**Synthesis of Potassium Butyl Xanthate,  $\text{KS}_2\text{COCH}_2\text{CH}_2\text{CH}_2\text{CH}_3$ .** Pulverized KOH 1.4 g (0.025 mol) was dissolved in 100 mL of butanol. After the solution was cooled to room temperature in an ice bath, 1.1 mL of  $\text{CS}_2$  (0.025 mol) was added dropwise over a period of 30 min. A yellow sticky precipitate appeared after about half of the  $\text{CS}_2$  was added. The mixture was stirred vigorously for an hour and filtered by suction. The yellow precipitate was washed several times with *n*-butanol until the pH of the washing solution was neutral. The precipitate was finally washed with diethyl ether and dried in a desiccator containing KOH; mp 243 °C dec, turning to orange-yellow. <sup>13</sup>C NMR ( $\text{CD}_3\text{CN}$ ):  $\delta$  = 73.0 (s), 32.3 (s), 20.6 (s), 14.8 (s) ppm. <sup>1</sup>H NMR ( $\text{CD}_3\text{OD}$ ):  $\delta$  = 0.95 (t,  $J_{\text{H-H}}$  = 8.2 Hz), 1.48, 1.72 (m, m;  $J_{\text{H-H}}$  = 7.4 Hz,  $J_{\text{H-H}}$  = 7.6 Hz), 4.39 (t,  $J_{\text{H-H}}$  = 6.4 Hz) ppm. Anal. Calcd for  $\text{KS}_2\text{OC}_4\text{H}_9$ : C, 31.88; H, 4.82. Found: C, 31.92; H, 4.64.

**Synthesis of Bis(tris-(2-cyanoethyl)phosphine)(*O*-Methyl dithiocarbonyl)gold(I),  $(\text{CEP})_2\text{AuS}_2\text{COCH}_3$ , **1**.**  $\text{CEP}_2\text{Cl}$ , 40 mg (0.065 mmol), was dissolved in 5 mL of  $\text{CH}_3\text{CN}/\text{CH}_3\text{OH}$  (3/2 by vol). Then 11 mg of  $\text{AgNO}_3$  (0.065 mmol) was added in one portion. The resultant mixture was stirred for 20 min in the dark, and the  $\text{AgCl}$  was filtered. To the filtrate was added 9.4 mg of the methyl xanthate ligand in one portion. The solution turned clear in about 15 min. After the mixture was stirred for 2 h, the solvent was partially evaporated under reduced pressure, and ethyl ether was added until a trace amount of cloudiness was formed. A light yellow crystalline product was obtained after keeping the mixture overnight in a freezer; mp 98–100 °C.

**Synthesis of Bis(tris-(2-cyanoethyl)phosphine)(*O*-ethyl dithiocarbonyl)gold(I),  $(\text{CEP})_2\text{AuS}_2\text{COCH}_2\text{CH}_3$ , **2**.**  $\text{CEP}_2\text{AuCl}$ , 40 mg (0.065 mmol), was dissolved in 5 mL of  $\text{CH}_3\text{CN}/\text{CH}_3\text{OH}$  (3/2 by vol), and 11 mg of  $\text{AgNO}_3$  (0.065 mmol) was added in one portion. The resultant mixture was stirred for 1 h in the dark, and the  $\text{AgCl}$  was removed by filtration. To the filtrate was added 10.4 mg of the ethyl xanthate ligand in one portion. After the mixture was stirred for 3 h, the solvent was reduced by half in vacuum. Diethyl ether was added until a permanent precipitate was observed. Yellow flakes were obtained after keeping the solution overnight in a refrigerator. Slow effusion of acetone into benzene gave yellow crystals suitable for X-ray measurement over a 2-week period; mp 111–113 °C.

**Synthesis of Bis(tris-(2-cyanoethyl)phosphine)(*O*-*n*-butyl dithiocarbonyl)gold(I),  $(\text{CEP})_2\text{AuS}_2\text{COCH}_2\text{CH}_2\text{CH}_2\text{CH}_3$ , **3**.**  $\text{CEP}_2\text{AuCl}$ , 100 mg (0.16 mmol), was dissolved in 5 mL of  $\text{CH}_3\text{CN}/\text{CH}_3\text{OH}$  (3/2 by vol). Then 27.5 mg of  $\text{AgNO}_3$  (0.16 mmol) was added in one portion. The resultant mixture was stirred for 20 min in the dark, and the  $\text{AgCl}$  precipitate was filtered. To the filtrate was added 30.4 mg of the butyl xanthate ligand in one portion and the mixture stirred for 3 h under  $\text{N}_2$ . The solvent was then reduced by half in vacuum, and diethyl ether was added until a permanent precipitate was observed. Yellowish flakes were obtained after keeping the solution overnight in a freezer. Slow diffusion

of diethyl ether into MeOH solution gave yellow crystals suitable for X-ray measurements; mp >225 °C.

**Synthesis of Bis(triphenylphosphine)(*O*-ethyl dithiocarbonyl)gold(I),  $(\text{Ph}_3\text{P})_2\text{AuS}_2\text{COCH}_2\text{CH}_3$ , **4**.** To 100 mg of  $(\text{Ph}_3\text{P})_2\text{AuCl}$  (0.13 mmol) was added 0.13 mmol of  $\text{AgNO}_3$  in one portion, and the resulting mixture was stirred for an hour in the dark. After the  $\text{AgCl}$  precipitate was filtered off, 21.1 mg of the ethyl xanthate ligand (0.13 mmol) was added in one portion. The solution was stirred for 3 h, and the solvent was reduced by half. Diethyl ether was added until a permanent precipitate was obtained, and the solution was kept overnight in a refrigerator. The yellow crystals obtained were recrystallized from  $\text{CH}_2\text{Cl}_2/\text{Et}_2\text{O}$  mixture. Yield: 87 mg (78%). Single crystals suitable for X-ray studies were grown by slow diffusion of diethyl ether into a  $\text{CH}_2\text{Cl}_2$  solution; mp 164–165 °C. Anal. Calcd C, 55.58; H, 4.15. Found: C, 56.28; H, 4.06.

**X-ray Structural Determination.** The X-ray structural determination was conducted on a Nicolet R3m/E diffractometer (SHELXTL 5.1) using the procedure described previously.<sup>14</sup> Unit cell constants for the compounds **2** and **4** were determined from 25 machine-centered reflections. Data were collected using graphite-monochromated  $\text{Mo K}\alpha$  radiation ( $\lambda = 0.71073 \text{ \AA}$ ) at room temperature. Intensity data of compound **2** were collected for 4078 unique reflections ( $+h, +k, \pm l$ ) with  $4^\circ < 2\theta < 45^\circ$  by using  $\omega$ -scanning technique. The data was corrected for Lorentz and polarization effects and for absorption by empirical methods based on azimuthal scans of four reflections. Automatic lattice determination for compound **2** predicted an orthorhombic crystal system. However, due to the absence of symmetry on *a* and *b*-axis photographs, the monoclinic system was assumed. Systematically absent reflections of  $l = 2n + 1$  in the  $00l$  and  $k0l$  zones indicated space group  $P2_1/c$  (No. 14). The choice was confirmed by the subsequent successful solution and refinement of the structure. Refinement of 143 parameters using 2989 reflections with  $F_o^2 > 3\sigma(F_o^2)$  converged to a conventional *R* value of 0.0325 with a goodness-of-fit indicator of 1.017. The structure was solved by direct methods. All non-hydrogen atoms were refined with anisotropic thermal parameters. Hydrogen atoms were placed in idealized positions ( $\text{C-H} = 0.96 \text{ \AA}$ ,  $U(\text{H}) = 1.2U_{\text{eq}}(\text{C})$ ). Data for compound **4** were corrected for Lorentz and polarization effects. The absorption correction was applied to the isotropic model using the program Diffabs.<sup>15</sup> Compound **4** crystallizes in the triclinic system. The space group is  $P\bar{1}$  (No. 2) as confirmed by the successful refinement of the structure. Refinement of 403 parameters using 3825 reflections ( $h, \pm k, \pm l$ ) with  $F_o^2 > 3\sigma(F_o^2)$  converged to a conventional *R* value of 0.0273 ( $R_w = 0.0269$ ) with a goodness-of-fit indicator of 1.229.

**Computational Details.** Extended Hückel (EH) calculations were performed on Macintosh IIfx computer using a molecular modelling CAChe software package.<sup>5</sup> Energy minimization was conducted using the MM2 program, which is included in the CAChe software, prior to running the EH calculation. The orbital energy and exponent parameters used in the EH calculation were obtained from Pyykkö's work and correspond to relativistic values.<sup>12c</sup> Charge iteration was used such that the charge on  $H_{\text{H}}$  was linearly related to the charge of the species. For *p*- and *d*-orbital parameters the weighted average of the low and high angular momentum values were used to satisfy the CAChe criteria. In the calculation,  $\text{PH}_3$  was used as the P-donor and methyl xanthate as the S-donor ligand. For the  $(\text{PH}_3)_2\text{Au}^+$  complex, the initial model was constructed as a linear geometry. The structure was then optimized using the MM2 program of the CAChe system. The optimized geometry also provides, as expected, a linear geometry. The P–Au–P angle of the optimized structure was slowly bent and the EH calculation performed at each bent geometry. The axis definition in the EH calculation is consistent throughout the bending procedure. The molecular plane is the *xz*-plane, and the *x*-axis bisects the molecule. The molecular modeling for  $[(\text{PH}_3)_2\text{AuS}_2\text{COCH}_3]$  was constructed by using crystallographic data for compounds **2** and **4**.

## Results

**Structural Determination.** Crystallographic data for the compounds  $(\text{CEP})_2\text{AuS}_2\text{COCH}_2\text{CH}_3$ , **2**, and  $(\text{Ph}_3\text{P})_2\text{AuS}_2\text{COCH}_2\text{CH}_3$ , **4**, are recorded in Table 1. Atomic positional and thermal parameters for **2** and **4** are given in Tables 2 and 3. Significant bond lengths and angles for **2** and **4** are given in Table 4. In Figures 1 and 2 the structures of compounds **2** and **4** are shown, respectively. In compound **2**, the Au atom is bound strongly with the two P atoms of the CEP ligand. The average

(14) Foyt, D. C. *Comput. Chem.* **1981**, *5*, 49.

(15) Walker, N.; Stuart, D. *Acta Crystallogr.* **1983**, *A39*, 158.

Table 1. Crystallographic Data

	AuS <sub>2</sub> P <sub>2</sub> O <sub>6</sub> C <sub>21</sub> H <sub>29</sub> , 2	AuS <sub>2</sub> P <sub>2</sub> O <sub>6</sub> OC <sub>39</sub> H <sub>35</sub> , 4
fw	704.5338	842.739
space group	P2 <sub>1</sub> /c (No. 14)	P1̄ (No. 2)
a, Å	11.538(2)	10.316(3)
b, Å	23.302(4)	13.058(2)
c, Å	11.565(1)	14.039(4)
α, deg	90.00	88.07(2)
β, deg	116.62(1)	74.40(2)
γ, deg	90.00	76.59(1)
V, Å <sup>3</sup>	2780.1(8)	1771.1(7)
Z	4	2
d <sub>calc</sub> , g/cm <sup>3</sup>	1.483	1.581
μ(Mo Kα), cm <sup>-1</sup>	55.63	43.74
radiation (λ, Å)	graphite monochromated Mo Kα	(0.71073)
temp, K	293	293
transm factor		
max	0.974	0.973 <sup>c</sup>
min	0.447	0.837 <sup>c</sup>
R, R <sub>w</sub> <sup>b</sup>	0.0325, 0.0318	0.0273, 0.0269

<sup>a</sup>  $R = \sum ||F_o| - |F_c|| / \sum |F_o|$ . <sup>b</sup>  $R = [\sum w^{1/2}(|F_o| - |F_c|)] / \sum w^{1/2}|F_o|$ ;  $w^1 = [\sigma^2(|F_o|) + g|F_o|^2]$ . <sup>c</sup> Absorption correction was performed using the Diffabs program.<sup>15</sup>

Table 2. Atomic Coordinates (×10<sup>4</sup>) and Isotropic Thermal Parameters (Å<sup>2</sup> × 10<sup>3</sup>)<sup>a</sup> for [Au(CEP)<sub>2</sub>(S<sub>2</sub>COCH<sub>2</sub>CH<sub>3</sub>)<sub>2</sub>], 2

atom	x	y	z	U <sub>iso</sub> <sup>b</sup>
Au	3654(1)	1730(1)	5519(1)	32(1)
S(1)	2686(2)	2784(1)	4865(2)	45(1)
S(2)	3745(2)	2712(1)	6785(2)	35(1)
P(1)	5798(2)	1601(1)	4061(2)	28(1)
P(2)	1675(2)	1284(1)	6662(2)	27(1)
O(1)	3189(5)	3660(2)	6039(4)	41(2)
N(1)	5339(9)	-24(3)	3078(9)	92(5)
N(2)	8062(8)	283(3)	6037(7)	69(4)
N(3)	7436(8)	3693(3)	3712(8)	83(4)
N(4)	894(8)	-630(3)	9047(7)	73(4)
N(5)	-132(7)	1321(4)	3282(6)	65(3)
N(6)	-1214(7)	2522(4)	10660(6)	69(3)
C(1)	3191(6)	3087(3)	5869(6)	32(3)
C(2)	2717(8)	4047(3)	5338(7)	53(4)
C(3)	2894(10)	4638(4)	5675(9)	71(5)
C(4)	6169(7)	1434(3)	2364(6)	40(3)
C(5)	5308(7)	986(3)	2181(7)	46(3)
C(6)	5345(8)	412(4)	2674(8)	53(4)
C(7)	6647(7)	1028(3)	4462(6)	34(3)
C(8)	6710(7)	1110(3)	5749(6)	43(3)
C(9)	6834(6)	2229(3)	3865(6)	36(3)
C(10)	6362(6)	2756(3)	3423(6)	38(3)
C(11)	6977(8)	3282(3)	3567(8)	53(4)
C(12)	7447(7)	649(3)	5950(7)	45(3)
C(13)	1838(6)	529(3)	6968(7)	40(3)
C(14)	584(7)	180(3)	7652(7)	48(3)
C(15)	730(7)	-281(3)	8434(7)	51(3)
C(16)	635(6)	1320(3)	5852(5)	34(3)
C(17)	1373(6)	1192(4)	4400(6)	41(3)
C(18)	519(7)	1258(3)	3768(6)	42(3)
C(19)	619(7)	1556(3)	8287(6)	38(3)
C(20)	351(7)	2197(3)	8316(6)	41(3)
C(21)	-533(7)	2384(3)	9639(7)	45(3)

<sup>a</sup> Estimated standard deviations in the least significant digits are given in parentheses. <sup>b</sup> The equivalent isotropic U is defined as one-third of the trace of the U<sub>ij</sub> tensor.

Au-P distance is 2.308 Å. The Au-S distances are rather long 2.745 and 2.934 Å. However, the large distortion in the P-Au-P interligand angle (145.3°) from a linear geometry is a clear indication of a weak Au-S covalent interaction in the molecule. In compound 4, which contains an arylphosphine (Ph<sub>3</sub>P), the interligand P-Au-P angle decreases further to 130.1°, and as a result the Au-S distance is significantly shorter, 2.53 Å, than in compound 2. The S atom closest to the Au atom in 4 deviates from the P-Au-P plane only by about 6°. The larger deviation has been observed for compound 2 (25°).

Table 3. Atomic Coordinates (×10<sup>4</sup>) and Isotropic Thermal Parameters (Å<sup>2</sup> × 10<sup>3</sup>)<sup>a</sup> for (Ph<sub>3</sub>P)<sub>2</sub>AuS<sub>2</sub>COCH<sub>2</sub>CH<sub>3</sub>, 4

atom	x	y	z	U <sub>iso</sub> <sup>b</sup>
Au(1)	9108(1)	1566(1)	2595(1)	35(1)
S(1)	11486(2)	1943(1)	1979(1)	48(1)
S(2)	9594(2)	3040(2)	809(2)	73(1)
P(1)	7539(2)	2995(1)	3557(1)	34(1)
P(2)	8891(2)	-132(1)	2390(1)	33(1)
O(1)	12114(4)	3280(3)	689(3)	54(2)
C(1)	11062(6)	2823(5)	1120(4)	41(2)
C(2)	11937(8)	4032(6)	-74(7)	79(4)
C(3)	13258(10)	4309(8)	-515(8)	109(5)
C(10)	7065(6)	2724(4)	4876(4)	36(2)
C(11)	6874(7)	1732(5)	5154(5)	46(3)
C(12)	6500(8)	1496(6)	6141(5)	62(3)
C(13)	6324(8)	2240(6)	6872(5)	67(3)
C(14)	6533(9)	3227(6)	6596(5)	68(4)
C(15)	6873(7)	3477(5)	5617(5)	54(3)
C(20)	8027(6)	4260(4)	3529(4)	37(2)
C(21)	7165(7)	5208(5)	3401(5)	50(3)
C(22)	7549(8)	6148(5)	3447(5)	60(3)
C(23)	8784(8)	6149(5)	3648(5)	57(3)
C(24)	9661(8)	5218(5)	3753(6)	62(3)
C(25)	9295(7)	4270(5)	3685(5)	52(3)
C(30)	5888(6)	3329(4)	3239(4)	33(2)
C(31)	4631(7)	3567(5)	3948(5)	45(3)
C(32)	3400(7)	3790(5)	3681(5)	53(3)
C(33)	3396(7)	3766(5)	2698(5)	49(3)
C(34)	4642(8)	3542(6)	2003(5)	63(3)
C(35)	5879(7)	3300(5)	2255(5)	56(3)
C(40)	8492(6)	-733(4)	3599(4)	33(2)
C(41)	7220(6)	-951(5)	4038(5)	43(3)
C(42)	6940(8)	-1323(5)	5002(5)	54(3)
C(43)	7941(8)	-1496(5)	5505(5)	57(3)
C(44)	9210(8)	-1282(5)	5077(5)	53(3)
C(45)	9498(7)	-912(5)	4127(5)	48(3)
C(50)	10386(6)	-1090(4)	1665(4)	34(2)
C(51)	11353(7)	-748(5)	929(5)	50(3)
C(52)	12502(8)	-1454(7)	375(5)	63(3)
C(53)	12697(8)	-2511(7)	559(6)	67(4)
C(54)	11734(8)	-2872(6)	1279(5)	65(3)
C(55)	10568(7)	-2163(5)	1828(5)	55(3)
C(60)	7435(6)	-204(4)	1905(4)	34(2)
C(61)	7490(7)	-970(5)	1228(5)	48(3)
C(62)	6338(7)	-991(6)	910(5)	57(3)
C(63)	5129(7)	-245(6)	1263(5)	55(3)
C(64)	5067(7)	523(6)	1934(5)	54(3)
C(65)	6227(6)	553(5)	2245(4)	42(2)

<sup>a</sup> Estimated standard deviations in the least significant digits are given in parentheses. <sup>b</sup> The equivalent isotropic U is defined as one-third of the trace of the U<sub>ij</sub> tensor.

Table 4. Selected Bond Distances (Å) and Bond Angles (deg) for Compounds 2 and 4

2		4	
Au-P(1)	2.306(1)	Au-P	2.349(1)
Au-P(2)	2.310(2)	Au-P(2)	2.315(2)
Au-S(2)	2.745(2)	Au-S(1)	2.530(2)
Au-S(1)	2.934(2)	Au-S(2)	3.112(2)
S(1)-C(1)	1.671(8)	S(1)-C(1)	1.710(7)
S(2)-C(1)	1.703(8)	S(2)-C(1)	1.646(7)
C(1)-O(1)	1.350(8)	C(1)-O(1)	1.350(8)
O(1)-C(2)	1.470(11)	O(1)-C(2)	1.448(10)
C(2)-C(3)	1.469(12)	C(2)-C(3)	1.460(13)
P(1)-Au-P(2)	145.3(1)	P(1)-Au-P(2)	130.1(1)
S(1)-Au-P(1)	102.36(1)	S(1)-Au-P(1)	110.8(1)
S(1)-Au-P(2)	97.51(1)	S(1)-Au-P(2)	118.1(1)
S(1)-C(1)-S(2)	124.1(4)	S(1)-C(1)-S(2)	124.5(4)
S(2)-C(1)-O(1)	113.1(6)	S(1)-C(1)-O(1)	111.3(5)
S(1)-C(1)-O(1)	122.8(6)	S(2)-C(1)-O(1)	124.1(5)
C(1)-O(1)-C(2)	120.2(7)	C(1)-O(1)-C(2)	118.5(6)
O(1)-C(2)-C(3)	107.4(9)	O(1)-C(2)-C(3)	108.4(7)

**Spectroscopic Studies.** Absorption spectra of the ligands Me, Et and Bu-xanthates in AN solution are shown in Figure 3. A high energy (HE) band is observed at ca. 308 nm for all three

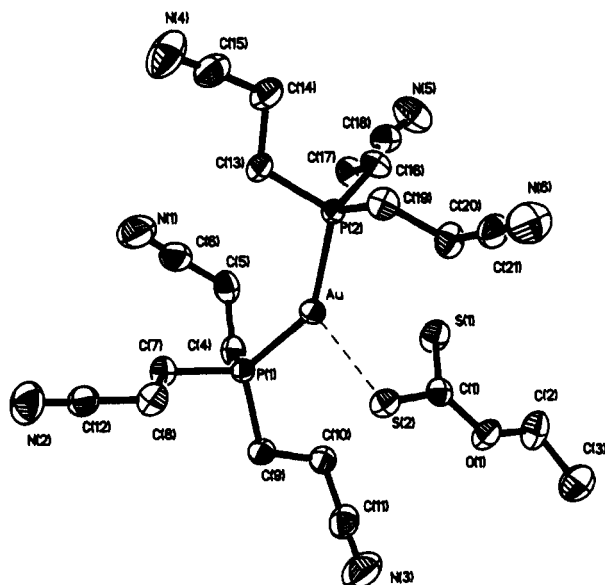


Figure 1. Thermal ellipsoid drawing of 2, with ellipsoids at the 50% probability level.

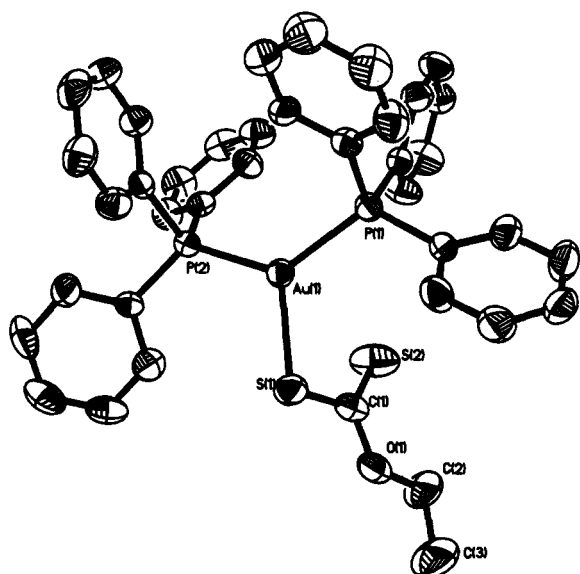


Figure 2. Thermal ellipsoid drawing of 4, with ellipsoids drawn at the 50% probability level.

ligands with an extinction coefficient value of  $(1.0\text{--}2.5) \times 10^4 \text{ M}^{-1} \text{ cm}^{-1}$ . The energy position of this band shows little variation among the ligands ( $\pm 2 \text{ nm}$ ). At higher concentrations a low-energy (LE) weak band appears ( $\epsilon \sim 50 \text{ M}^{-1} \text{ cm}^{-1}$ ). The position of this LE band is affected by substituents ( $\pm 10 \text{ nm}$ ) on the xanthate ligands. In the Et- and Bu-xanthates, a red shift has been observed in AN solution in the LE band. Due to limited solubility in various solvents the Me- and Et-xanthates were found unsuitable for more detailed solvent dependent studies. The solvent dependent properties of the LE band as observed in the Bu-xanthate ligand are presented in Table 5. A blue shift in H-bonding solvents and a red shift in electron donating solvents are characteristics of the LE band. In MeOH, for example, the LE band shifts to 380 nm when compared to the 394-nm value found in pyridine solution. The high-energy band observed at ca. 308 nm is affected little by these solvents.

Absorption spectra of the complexes 1–4 are compared in Figure 4. Both the high- and low-energy bands of the free ligands are observed in the absorption spectra of the complexes. Compared to the free ligands, the HE intense band shows a slight blue shift upon complexation. However, the energy position of this HE band shows little variation among the complexes. Like the ligands

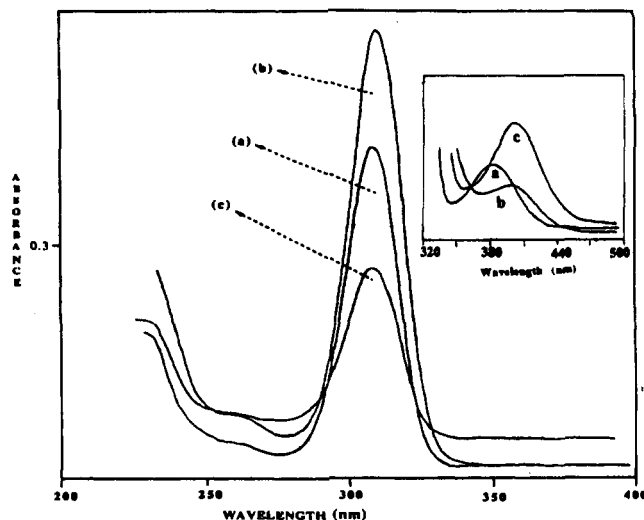


Figure 3. Electronic absorption spectra of the xanthate ligands in acetonitrile solution: (a)  $2.8 \times 10^{-5} \text{ M}$  Me-xanthate; (b)  $2.3 \times 10^{-5} \text{ M}$  Et-xanthate; (c)  $2.8 \times 10^{-5} \text{ M}$  Bu-xanthate. Inset shows the low-energy band at higher concentration. The transition energies and solvent dependent values for the Bu-xanthate ligand are shown in Table 5.

Table 5. Electronic Absorption Data for the Xanthate Ligands and Complexes

	solvent <sup>1</sup>	$\lambda_{\text{max}}$ , nm	$\epsilon$ , $\text{M}^{-1} \text{ cm}^{-1}$
KS <sub>2</sub> COMe	MeOH	308	16300
		382	$\sim 50$
KS <sub>2</sub> COEt	AN	308	24000
		394	$\sim 50$
KS <sub>2</sub> COBu	AN	308	10000
		402	20
		400	
		394	
		382	
(CEP) <sub>2</sub> S <sub>2</sub> COMe (1)	AN	304	13100
		373	100
(CEP) <sub>2</sub> S <sub>2</sub> COEt (2)	AN	305	10500
		392	<i>a</i>
(CEP) <sub>2</sub> S <sub>2</sub> COBu (3)	AN	304	13000
		375	40
		306	16800
(Ph <sub>3</sub> P) <sub>2</sub> S <sub>2</sub> COEt (4)	AN	375	$\sim 50$

<sup>a</sup> Solid spectra obtained by using a Nujol mull of the complex on filter paper. Nujol alone on filter paper was used as a reference.

the LE weak band ( $\epsilon = 50 \text{ M}^{-1} \text{ cm}^{-1}$ ) also appears in the near-UV region. This LE band shows a substantial blue shift in the complexes when compared to the spectra of the free ligands. For example, the band in compound 1 blue shifts by ca. 650  $\text{cm}^{-1}$  relative to the methyl xanthate ligand. The LE band is absent in the absorption spectra of the starting gold compounds, CEP<sub>2</sub>-AuCl and (Ph<sub>3</sub>P)<sub>2</sub>AuCl, whose lowest absorption bands are observed at wavelengths less than 280 nm.

Emission spectra of compounds 1, 2, and 3 are presented in Figure 5 in solid (top) and solution (bottom), respectively. A broad asymmetric band has been observed for the compounds centering at ca. 490. All three compounds emit strongly in acetonitrile solution. No shift in emission energy has been observed between the solid state and solution spectra. However, compared with 1, compound 3 loses its capacity to emit with time. In one experiment the emission intensity from compound 3 has been decreased by 80% over a 15-min period. Compound 4 does not emit at room temperature while the free anionic ligands show a very weak structured emission. The excitation spectra of complexes 1–3 are compared in Figure 6. The excitation spectra closely resemble the absorption spectra of the compounds in the low-energy region. The emission lifetimes for the solids are in nanosecond range ( $< 10 \text{ ns}$ ).

**Electronic Structure.** The EH parameters used in the calcula-

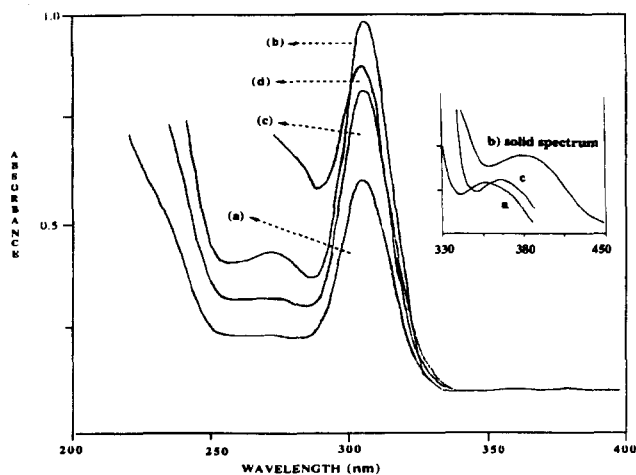


**Figure 4.** Electronic absorption spectra of complexes **1**, **2**, **3** and **4** in acetonitrile solution. (a)  $5.2 \times 10^{-5}$  M of **1**; (b)  $1.1 \times 10^{-4}$  M of **2**; (c)  $7.1 \times 10^{-5}$  M of **3**; (d)  $5.3 \times 10^{-5}$  of **4**. Inset shows the low-energy band at higher concentration. The spectrum shown, in the inset, for compound **2** is a solid-state spectrum recorded by using a dispersion of Nujol mull on filter paper. Nujol alone was used as a reference. The solid-state spectrum was recorded because of solubility limitations.

tion are listed in Table 6. Electronic structures of the  $(\text{PH}_3)_2\text{-Au}^+$  fragment are shown in Figure 7. The MM2 optimized structure of the fragment has a linear geometry. The calculated Au-P bond distance of 2.40 Å is slightly longer than the values obtained from the crystallographic data (Table 4). The calculated P-H distance is 1.43 Å, and the H-P-H angle is 98.9°. The EH calculation conducted on the optimized fragment provides a  $3\sigma_g$  HOMO which consists mainly of  $5d_{z^2}$  and  $6s$  contributions from the metal (80% and 12% respectively) and phosphorus (8%  $p_z$ ), the latter signifying P  $\rightarrow$  Au  $\sigma$ -donation. The  $2\sigma_u$  SHOMO also consists of Au  $p_z$  and the P lone pairs. These bonding features in the linear geometry are also recognized in the Mulliken populations (Table 7) obtained from the Fenske-Hall calculation. Populations of 0.82 and 0.42 on s and p valence orbitals of Au respectively are evidence of participation in the AuP bond formation by these orbitals.<sup>18</sup> The LUMO is degenerate and consists of P and Au  $\pi$  contributions (50% and 22%, respectively).

When the P-Au-P angle is bent, the  $\sigma$ -interaction between the P  $p_z$  and Au( $d_{z^2}$ ,  $6s$ ) orbital decreases and the hybridized ( $p_z$ ,  $p_x$ ) orbital of P interacts with the  $d_{xz}$  orbital of the gold in the  $\sigma$  Au-P bonding. The P  $p_x$  contribution in the hybridized orbital becomes substantial with increased bending. As a consequence of this interaction the  $d_{xz}$  orbital is destabilized and the  $5d_{z^2}$  orbital is stabilized. At a P-Au-P interligand angle of about 168°, a crossing of the  $5d_{xz}$  and  $5d_{z^2}$  energy levels takes place and the  $5d_{xz}$  becomes the HOMO. These changes are shown in Figure 8. At a P-Au-P interligand angle of 120°, the angle used in the xanthate calculation below, the HOMO consists of 44% Au  $d_{xz}$ , and 39% P  $p_z$  and  $p_x$  contributions.

The electronic structure of the  $(\text{PH}_3)_2\text{AuS}_2\text{COCH}_3$  complex obtained from the EH calculation is shown in Figure 9. For the calculation conducted using the crystallographic data of **4** (Au-S distance 2.53 Å) the HOMO consists of an Au  $5d_{xz}$  contribution (15%) and S  $p_z$  (67%). When the Au-S distance is increased to 2.74 Å (as found in compound **2**) the metal contribution in the HOMO decreases to 5%. The HOMO-LUMO gap also increases with an increase in the Au-S separation. According to Mulliken population analysis obtained from the Fenske-Hall calculation

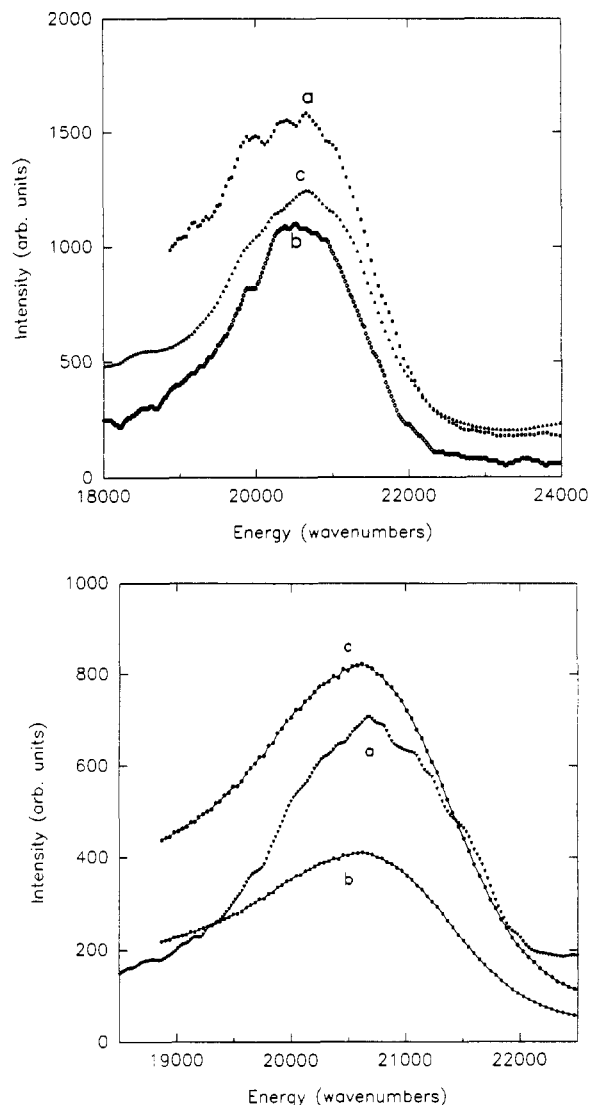


**Figure 5.** Top: Solid state emission spectra of the complexes at room temperature: (a) **1**; (b) **2**; (c) **3**. The spectra are corrected for instrumental responses. Emission areas are held arbitrarily constant to facilitate viewing. The emission intensity of compound **3** decreases with time. In one experiment the emission intensity decreased by 80% in 15 min time indicating photodegradation of this complex. Bottom: Solution spectra of (a) **1**, (b) **2**, and (c) **3** in acetonitrile.

**Table 6.** Extended Hückel Relativistic Parameters<sup>a</sup> Obtained from Reference 12c

orbital	$-H_{ij}$ , eV	Slater exponent
Au 6s	7.94 (9.23)	2.12 (1.75)
Au 6p	3.47 (3.52)	1.50 (1.36)
Au 5d	12.37 (11.8)	3.47 (3.56)
P 3s	19.30 (16.15)	1.82 (1.82)
P 3p	9.52 (10.49)	1.48 (1.48)
S 3s	24.14 (20.2)	2.04 (2.03)
S 3p	11.58 (10.36)	1.69 (1.69)
O 2s	34.08 (28.48)	2.19 (2.19)
O 2p	16.76 (13.62)	2.02 (2.02)
C 2s	19.39 (16.59)	1.58 (1.58)
C 2p	11.03 (11.26)	1.43 (1.45)
H 1s	13.61 (13.61)	1.00 (1.2)

<sup>a</sup> Data in parentheses are default parameters included in the CAChe system.

- (16) Assefa, Z.; Staples, R. J.; Fackler, J. P., Jr.; *Acta Crystallogr.*, to be submitted for publication.  
 (17) Streuli, C. A. *Anal. Chem.* **1960**, *31*, 985. Cotton, F. A., Darensbourg, D. D.; Ilsley, W. H. *Inorg. Chem.* **1981**, *20*, 578.  
 (18) Schwerdtfeger, P.; Dolg, M.; Schwarz, W. H. E.; Bowmaker, G. A.; Boyd, P. D. W. *J. Chem. Phys.* **1989**, *91*, 1762.

(Table 7), the gross orbital population on the Au 6p orbital nearly doubles when the xanthate ligand is introduced into the bent  $\text{P}_2\text{Au}^+$  fragment. A significant decrease in the electron density on the S p-orbitals has also been noted, indicating transfer of electron density from the sulfur to the gold center.

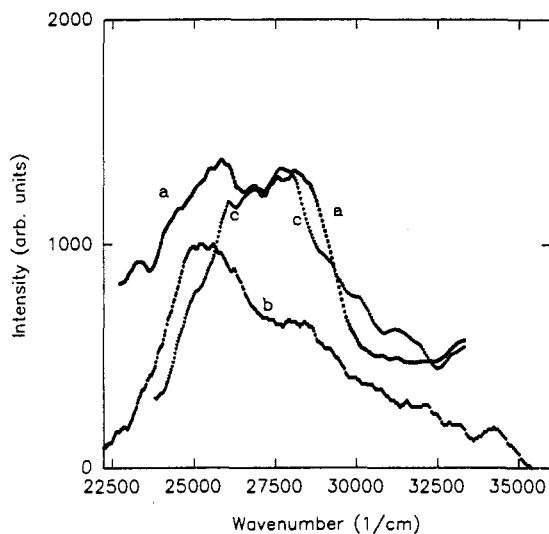


**Figure 6.** Comparison of excitation spectra of the complexes (a) 1, (b) 2, and (c) 3. Note that the excitation bands for all the complexes peak at the LE absorption band shown in the inset of Figure 4.

### Discussion

**Structural Comparison.** In addition to the Et-xanthate complex of the cation  $(\text{CEP})_2\text{Au}^+$  with the structure shown in Figure 1, both the Me- and Bu-xanthate adducts (compounds 1 and 3) of the cation have also been characterized crystallographically.<sup>16</sup> Both compounds are structurally similar to compound 2. While the Au-S distances and the P-Au-P angles in compounds 1-3 are almost the same, structural comparison of these compounds with the compound  $(\text{Ph}_3\text{P})_2\text{AuS}_2\text{COEt}$ , 4, indicates a much greater asymmetry in the Au-S bonding in the latter compound. The short Au-S distance in compound 4 (2.53 Å) is comparable to the value observed in the three-coordinate  $[(\text{Ph}_3\text{P})_2\text{AuSCN}]$

(2.47 Å).<sup>3</sup> The deviation of this S atom from the P-Au-P mean plane is 0.49 Å. The long Au-S distance in 4 is 3.112(2) Å, indicating no significant interaction of Au with this sulfur atom. In compound 2, the shorter Au-S distance is 2.745(2) Å and the deviation of the S atom from the P-Au-P mean plane is 1.08 Å. The longer Au-S distance is 2.934(2) Å. Thus a strong Au-S bonding interaction is not observed in 2. However, the presence of a weak interaction between the  $\text{CEP}_2\text{Au}^+$  unit and the xanthate ligands is evident as the P-Au-P angle is significantly reduced (145.5°) from a linear angle of 180°. In 2, which appears to be four-coordinate, both Au-S distances are intermediate to those in 4. The latter compound, 4, has a geometry around Au which approaches more closely a trigonal planar  $\text{AuP}_2\text{S}$  coordination. A similar trend, where  $(\text{Ph}_3\text{P})_2\text{Au}^+$  shows a smaller P-Au-P angle in three-coordinate complexes than does  $(\text{CEP})_2\text{Au}^+$ , has<sup>13</sup> been noted in previous studies. For example, in  $(\text{Ph}_3\text{P})_2\text{AuCl}$  the geometry<sup>2</sup> around Au is planar three-coordinate with a P-Au-P angle close to 120° and a short Au-Cl bonding. However, in the corresponding  $(\text{CEP})_2\text{AuCl}$  complex,<sup>13</sup> the P-Au-P angle is close to 180° with no Au-Cl interaction.

Accumulated data regarding Au-P bonding suggest that both good  $\sigma$ -donor and good  $\pi$ -accepting phosphines interact strongly with the metal center. Linear two-coordinate  $\text{P}_2\text{Au}^+$  complexes with good  $\sigma$ -donor phosphines have been noted to resist increased coordination while those with good  $\pi$ -accepting phosphines tend to form three- or four-coordinate complexes.<sup>2-4</sup> It is interesting to note a similar trend in this study, too. The CEP ligand which contains CN substituents separated from the P atom by two saturated carbon atoms has been shown to have an unusual  $\pi$ -acidity comparable to that of  $\text{Ph}_3\text{P}$ .<sup>17</sup> Although the CEP ligand is less bulky than the  $\text{Ph}_3\text{P}$ , the interligand P-Au-P angle in  $(\text{Ph}_3\text{P})_2\text{AuS}_2\text{COEt}$ , 4, is smaller than in 2. In accord with this reduced P-Au-P angle, the Au-S interaction, as inferred from the Au-S separation, is stronger in compound 4 than 2, suggesting

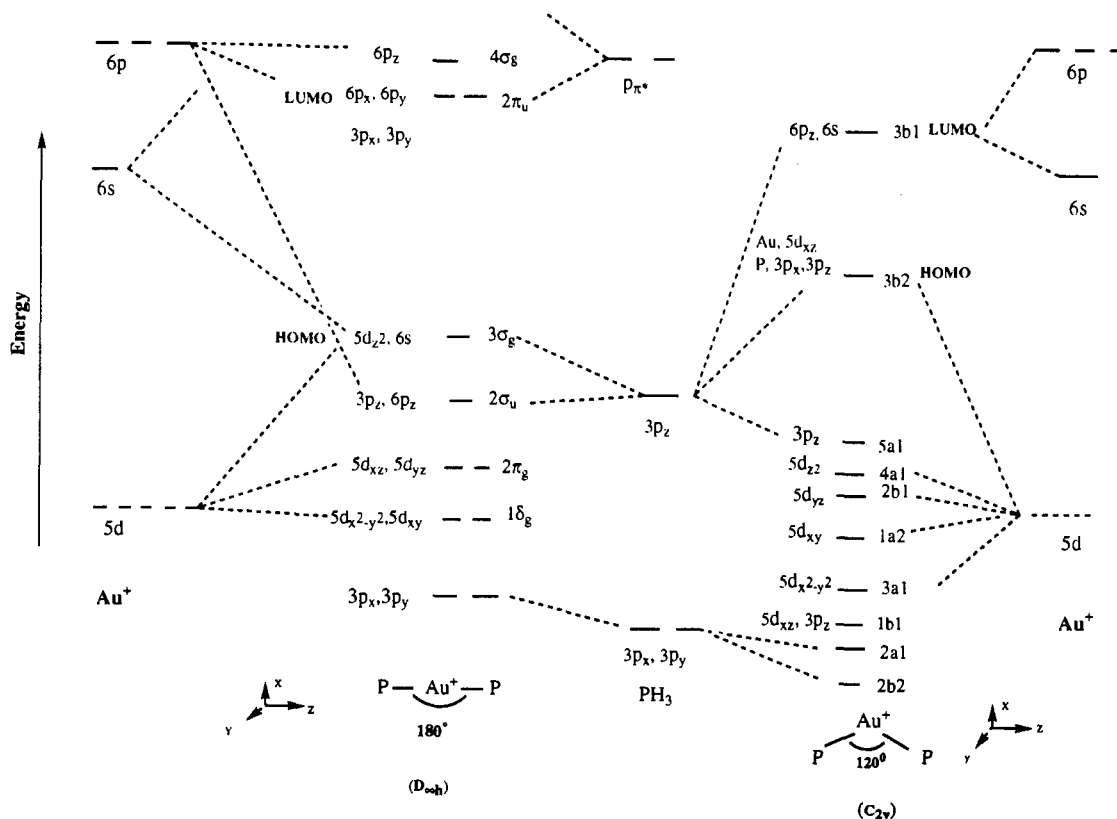


**Figure 7.** Electronic structure of the  $(\text{PH}_3)_2\text{Au}^+$  fragment in linear and bent geometries (shown as an orbital correlation diagram). The symmetry is approximated as  $D_{\infty h}$  in the linear and as  $C_{2v}$  in the bent geometries. The z-axis in the linear geometry is defined as the molecular axis and the x-axis bisects the molecule. The same axes definition was adopted in the bent geometry so as the xz-plane is the molecular plane. Orbital correlation is shown based on the correlation table adopted from ref 24. The  $D_{\infty h} \rightarrow C_{2v}$  "z  $\rightarrow$  y" case is used for our axes definition.

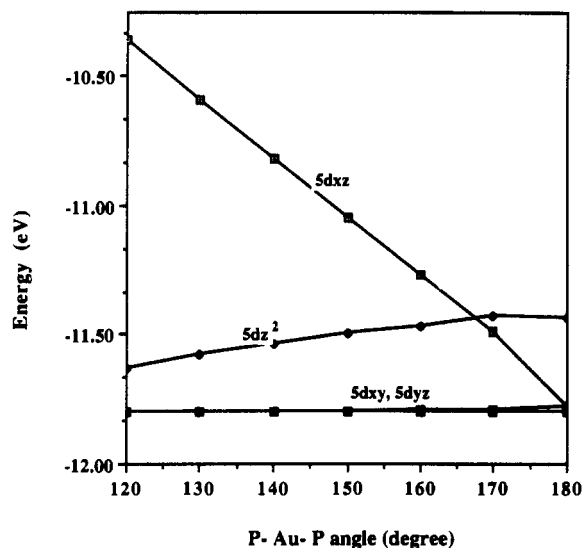


**Figure 8.** Correlation between the 5d orbital energies with the PAuP interligand angle. Note the stabilization of the  $5d_{z^2}$  orbital when the interligand angle decreases. Below  $168^\circ$  the  $5d_{z^2}$  orbital is not the HOMO and is replaced by a  $5d_{xz}$  orbital ( $d_{xz}$ ).

**Table 7.** Mulliken Population Analysis

atom	orbital	$(\text{PH}_3)_2\text{Au}^+$		
		P-Au-P ( $180^\circ$ )	P-Au-P ( $120^\circ$ )	$[(\text{PH}_3)_2\text{Au}]_2\text{S}_2\text{COCH}_3$
Au	6s	0.82	0.61	0.52
	6p	0.42	0.52	0.89
	x	-0.01	0.03	0.31
	y	-0.01	-0.01	0.14
	z	0.45	0.49	0.44
	5d	9.70	9.74	9.67
	$z^2$	1.78	1.86	1.85
	xy	2.0	1.99	1.96
	$x^2 - y^2$	2.0	1.99	1.98
	xz	1.97	1.92	1.92
	yz	1.95	1.97	1.96
P	3s	1.42	1.42	1.44
	3p	3.11	3.27	3.27
	x	0.91	1.30	1.28
	y	1.09	0.85	0.86
	z	1.11	1.12	1.13

that electronic factors are important in influencing the geometries of the complexes.

**Molecular Orbital Calculation.** Previous theoretical work<sup>18,19</sup> on linear  $[\text{P}_2\text{Au}^+]$  type complexes have indicated that gold 6s and  $6p_z$  orbitals are strongly involved in Au-P  $\sigma$ -bonding with minimal  $5d_{z^2}$  involvement. In a recent study, Au(5d) participation has been pointed out to be substantial due to relativistic effects as well as activation by phosphines.<sup>20</sup> The  $\sigma$ -donation by P into the Au 6s and  $6p_z$  orbitals has also been noted in the EH calculation conducted in this study on the linear  $(\text{PH}_3)_2\text{Au}^+$  fragment. As shown in Figure 7, the phosphorus  $3p_z$ , gold 6s interaction is recognized in the HOMO, and the  $3p_z$ ,  $6p_z$  interaction, in the SHOMO. When the P-Au-P angle is reduced, the metal 6s contribution in the HOMO diminishes and its contribution in the LUMO becomes substantial. In addition, the  $\sigma$ -interaction between the Au  $5d_{z^2}$  and P  $p_z$  orbitals in the linear geometry is replaced by the  $\sigma$ -interaction between the hybridized P  $3p_z$ ,  $3p_x$  and Au  $5d_{xz}$  orbitals. The interaction destabilizes the Au  $5d_{xz}$  orbital upon bending. Accordingly, the HOMO orbital in the bent geometry is at a higher energy level compared with the linear geometry. While the HOMO is destabilized, the LUMO

is stabilized with bending. As a consequence the HOMO-LUMO gap decreases.

The destabilization of the HOMO in the bent  $\text{P}_2\text{Au}^+$  fragment indicates that the metal center is better activated toward electron transfer from the metal to an incoming ligand. Similar destabilization of the metal  $d_{xz}$  orbital has been noted<sup>10,11,21</sup> in the  $d^{10}$  systems of  $\text{P}_2\text{Pt}$  and  $\text{P}_2\text{Ni}$ . Goddard, et al.<sup>10</sup> have noted that, with a decreased P-Pt-P angle, one of the Pt 5d orbitals ( $d_{yz}$ ) is destabilized and better activated toward electron donation to an incoming ligand. However, unlike the  $\text{Pt}^0$  complexes, oxidative addition reactions are not common with bis(phosphine)- $\text{Au}^+$  complexes. The +1 charge on the gold provides part of the explanation for the differences between the bis(phosphine)- $\text{Au}^+$  and  $-\text{Pt}^0$  complexes toward oxidative addition reactions. The theoretical result on the  $[(\text{PH}_3)_2\text{Pt}(\text{H}_2)]$  complex reported by Goddard et al.<sup>10</sup> does not show any net charge transfer from the Pt center to the hydrogen atoms even though the Pt is expected to have a net +2 charge in the full sense of oxidative addition reaction. Promotion to the  $d^9s^1$  configuration, which is preferred in the bent geometry, produces the interaction between the  $\text{P}_2\text{Pt}^0$  moiety and the incoming hydrogen atoms.

The interaction between the xanthate ligand and the  $\text{P}_2\text{Au}^+$  fragment can be explained by the changes taking place in the frontier orbitals of the  $\text{P}_2\text{Au}^+$  fragment. The destabilization of the  $5d_{xz}$  orbital in the bent geometry of the  $\text{P}_2\text{Au}^+$  fragment favors a back electron transfer from the metal to the incoming xanthate  $\pi^*$  orbital. On the other hand, the stabilization of the LUMO in the bent geometry (Figure 7) favors an electron transfer from the ligand HOMO to this empty orbital. Comparison of Au-S distances and P-Au-P angles in compounds 2 and 4 indicates that the shortest Au-S separation is observed in 4, which also has the smallest P-Au-P angle. Thus, both the back electron transfer from the metal center to the xanthate and the forward electron transfer from the xanthate HOMO to the metal center are favored with bending. However, the increased Mulliken charge on the metal center, as inferred from the population analysis (Table 7), indicates net electron density transfer from the xanthate to the metal. This can be observed most readily by comparing the populations in the 6p Au orbital before and after complexation. The increased population of the Au 6p orbital also indicates electron donation from the xanthate ligand to this orbital. This suggests that the forward electron transfer from the incoming xanthate to the  $\text{P}_2\text{Au}^+$  fragment LUMO dominates when compared to the back electron transfer from the metal  $d_{xz}$  orbital to the xanthate LUMO. In the  $(\text{PH}_3)_2\text{Pt}^0$  case an initial electron donation from the incoming ligand has been found to populate the Pt 6s orbital<sup>10,11</sup> rather than the 6p orbital as found in the gold complex. These results suggest that the  $(\text{PH}_3)_2\text{Au}^+$  moiety interacts preferentially with  $\pi$ -interacting ligands while, the  $(\text{PH}_3)_2\text{Pt}^0$  moiety interacts with  $\sigma$  donors. This tendency may be the reason that gold-phosphine complexes are known to resist oxidative addition while the Pt complexes readily add ligands oxidatively.

The extent of resonance  $\pi$ -electron donation by xanthate and other similar 1,1-dithiolates to a metal center has been analyzed previously by Fackler et al.<sup>22</sup> The structural data indicates the importance of resonance form I shown in Chart 1. The C1-O distance in both complexes (Table 4) is shorter than the C2-O distance, indicating a double bond character between the oxygen and C1 atoms. Resonance  $\pi$ -electron donation to the gold center is expected to weaken the S-C interaction. The weakening of the bond is evident both from structural and IR studies. Structurally, the S1-C1 distance is slightly longer in 4 than in 2. The IR data interpreted using previous assignments is consistent with this structural data where, the  $\nu_{\text{S-C}}$  stretching frequency observed at

(19) Mingos, D. M. P. *J. Chem. Soc., Dalton Trans.* **1976**, 1163.

(20) Schwerdtfeger, P.; Boyd, P. D. W. *Inorg. Chem.* **1992**, *31*, 327.

(21) Re, N.; Rosi, M.; Sgamellotti, A.; Floriani, C.; Guest, M., *J. Chem. Soc., Dalton Trans.* **1992**, 1821.

(22) Coucouvanis, D.; Fackler, J. P., Jr. *Inorg. Chem.* **1967**, *6*, 2047.

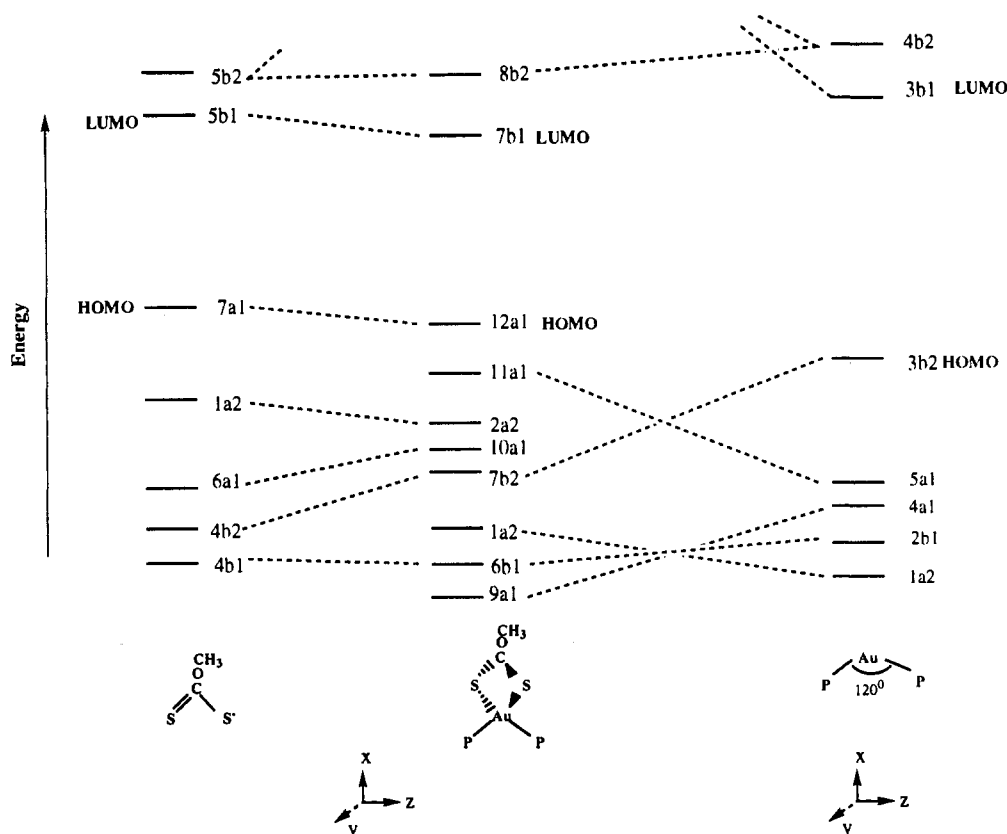
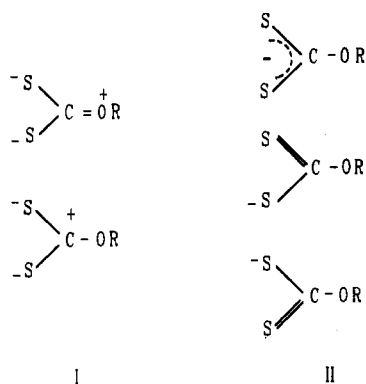


**Figure 9.** Electronic structure of the  $[(\text{PH}_3)_2\text{AuS}_2\text{COCH}_3]$  complex. The P-H distance was kept at 1.42 Å. The bond distances used for the other atoms were taken from the crystallographic data of **2**. Energy minimization with the MM2 program of the CAChe system was performed before running the extended Hückel calculation. The minimized structure has a much shorter Au-S distance (2.38 Å) than found crystallographically both in **2** and **4**. The relativistic parameters used in the extended Hückel calculation were taken from ref 12c. The weighted averages were used for p- and d-orbitals. The symmetry around the gold is assumed to be  $C_{2v}$ . The  $\text{P}_2\text{Au}^+$  fragment is placed in the  $xz$ -plane. The  $x$ -axis bisects the  $\text{PAuP}$  angle and passes through the center of xanthate ligand.

### Chart 1



802  $\text{cm}^{-1}$  in the ethyl xanthate ligand (potassium salt) decreases to 760 and 738  $\text{cm}^{-1}$  in compounds **2** and **4**, respectively. The C1-O distance in **2** is slightly longer than that in **4**. This suggests that the increased interaction between the gold and sulfur in **4** weakens the S-C1 interaction. Due to a decreased electron density on the C1, the oxygen atom would interact better with the C2 in compound **4** than in **2**. The IR band observed at 1130  $\text{cm}^{-1}$  in the free ligand corresponds to the C2-O stretch.<sup>22,23</sup> In the complexes **2** and **4**, this band shifts to higher frequencies (1155 and 1165  $\text{cm}^{-1}$ , respectively). A decrease in the  $\nu_{\text{C-S}}$  and an increase in the  $\nu_{\text{C}_2\text{-O}}$  stretching frequency from compound **2** to compound **4** is consistent with an increased electron donation of

the xanthate ligand to the more bent and thus better  $\pi$ -accepting Au center in **4**.

**Absorption Spectra.** Analysis of the photophysical properties of the xanthate ligands facilitates the assignments of the different transitions observed in the complexes. As mentioned earlier, resonance effects favoring forms I would lead to charge separation and thus unsaturation on the oxygen atom. Considerable delocalization occurs on the  $\text{CS}_2$  fragment. Thus, the ligands are expected to show absorption bands characteristic of  $\pi$ - $\pi^*$  and  $n$ - $\pi^*$  transitions. The intense absorption band (HE) exhibited by the free ligands at around 308 nm is assigned to  $\pi$ - $\pi^*$  transition. The assignment is based on extinction coefficient values and the energy of the band when compared with several other 1,1-dithiolate ligands (Table 5). The energy of this band shows little variation with solvent polarity. Substituents on the xanthate ligand also have little effect on the position of the band. Thus, the Me-, Et- and Bu-xanthates all show this HE band at about 308 nm with comparable intensity. In addition to this HE band, all the ligands show a weak band in the near-UV region. The lower extinction coefficient values as well as solvent dependent behavior of the LE band indicate that it corresponds to a  $n$ - $\pi^*$  transition. A substantial red shift in the LE band has been observed when the substituent electron-donating ability increases. For example, the band red shifts by 1300  $\text{cm}^{-1}$  in the Bu-xanthate when compared to the Me-xanthate ligand. Moreover, compared to electron-donating solvents such as pyridine, a blue shift in the LE band in H-bonding solvents such as MeOH has been observed.

The solvent and substituent effects on the LE band can be described in terms of the resonance properties discussed above. Electron donating substituents on the oxygen atom and basic solvents are expected to favor resonance forms with increased charge separation. The charge separation in forms I destabilize

(23) Watt, C. W.; McCormick, B. J. *Spectrosc. Chem. Acta*, **1965**, *21*, 753.  
 (24) Herzberg, G. *Molecular Spectra and Molecular Structure III. Electronic Spectra of Electronic Structure of Poly Atomic Molecules*; Nostrand: Princeton, NJ, 1966; p 576.

the n-orbital relative to forms II. In the presence of H-bonding solvents, the nonbonding orbitals on the S atoms are stabilized. Increased electron donation by the substituents on the oxygen atom is expected to destabilize the energy of the n-orbitals. Accordingly, the red shift in the  $n-\pi^*$  transition increases in the order Me-, Et-, and Bu-xanthate.

The absorption bands of the complexes are similar to those of the free ligands in terms of energy, extinction coefficient, and solvent-dependent properties. This indicates that the transitions center on the 1,1-dithiolate ligand. The similarities between the absorption properties of the ligands and the complexes simplifies assignments of the transitions observed in the complexes. Consistent with the MO calculation result, shown in Figure 9, the HE band of the complexes, which is observed at about 306 nm, is assigned<sup>25</sup> to a  $\pi-\pi^*$  transition ( $7b_2 \rightarrow 7b_1$ ) while the LE band corresponds to the ligand based  $n-\pi^*$  transition ( $12a_1 \rightarrow 7b_1$ ). Compared to bands in the free ligand, the intense HE band blue shifts slightly in the complexes while the LE band blue shifts significantly. The pattern of the absorption bands observed in the complexes indicate that the gold-phosphine moiety behaves as an electron-withdrawing group. This electron-withdrawing tendency of the  $P_2Au^+$  moiety is expected to stabilize the filled nonbonding orbital of the xanthate ligand. The high-energy (HE)  $\pi-\pi^*$  band is relatively unchanged upon complexation. This suggests that the Au-S interaction influences the ligand  $\pi^*$  and  $\pi$  orbitals to about the same degree. These results are consistent with well-known observations for  $n-\pi^*$  and  $\pi-\pi^*$  transitions in aromatic systems.<sup>26</sup>

**Luminescence Properties.** Compounds 1-3 luminesce in the solid state at room temperature. The luminescence observed in the complexes is associated with the  $n-\pi^*$  transition centering on the xanthate ligand. The assignment is based on the similar appearance of the lowest absorption band and the excitation spectrum. The short luminescence lifetimes and the relatively small Stokes shift between absorption and emission bands suggests that the emission is a fluorescence between singlet states. The structured nature of the emission band also suggests that a ligand-centered transition is responsible for the photoluminescence in these complexes, especially since no high-energy ( $>500\text{ cm}^{-1}$ ) metal-ligand vibrations are present in these complexes.

Additional evidence for these assignments comes from comparison of solid state emission with that of the solution spectra. In these xanthate compounds, which emit strongly in acetonitrile solution, no shift in emission energy is observed between the solid and solution spectra (Figure 5, top and bottom, respectively). This indicates that the Au-S interaction imposes minimal perturbation on the ligand orbitals as the Au-S separation is large in all three complexes. The luminescence result is thus consistent with a ligand centered transition.

Unlike 1-3, the triphenyl phosphine complex 4 is nonemissive in the visible spectral region at room temperature. The non emissiveness of 4 may be due to the stronger Au-S interaction observed in this compound. From the MO calculation, the HOMO in the complexes shows essentially a 1,1-dithiolate contribution. The LUMO, on the other hand, has a small contribution from the Au  $p_x$  orbital. The second unoccupied orbital, which is situated at a relatively small gap above the LUMO, has a large gold  $p_x$  contribution. With an increased Au-S interaction the Au  $6p_x$  contribution in the LUMO has been noted to increase, giving some ligand to metal CT character to the transition. Moreover, since compound 4 has a smaller P-Au-P interligand angle and is better activated to accept electron density, the LMCT state would be at a relatively lower level than in compounds 1-3. It is likely that thermal activation to the CT state may lead to a fast radiationless decay in compound 4, quenching the emission at higher temperatures. Compound 4 does show a weak yellowish emission when immersed in liquid  $N_2$  and irradiated with a hand-held UV lamp. Due to instrumental limitations we have not conducted temperature-dependent measurements on this compound and thus have not compared the emission behavior at low temperature with the room-temperature results.

**Conclusion.** The interaction between bis(phosphine)gold(I) complexes and incoming xanthate ligands has been correlated with the interligand P-Au-P angle. The structural and theoretical investigations reported here suggest that an increased bending of the P-Au-P angle activates the metal center and allows a strong bonding interaction with the xanthate. The xanthates behave as  $\pi$ -electron donors and populate principally the metal 6p orbitals. Thus the degree of electron density donation by the xanthates to the metal center is determined by the extent the P-Au-P angle bends. The PL properties of the complexes arise from a ligand centered  $n-\pi^*$  transition. The short emission lifetimes indicate the  $^1\pi^*$  state to be the principal emitting state. Bending the P-Au-P angle while sortening the Au-S distance increases the metal  $p_x$  contribution in the LUMO, providing some charge transfer character to the transition.

**Acknowledgment.** We would like to thank Dr. Nick Pace and Eric Hubert (Biochemistry and Biophysics at A&M University) for allowing us to use their emission spectrofluorometer for some of our samples. We acknowledge the financial support from the National Science Foundation (CHE 9300107) and the Welch Foundation. Lifetime and luminescence measurements were obtained at the Center for Fast Kinetics Research which is supported jointly by the NIH (Grant RR 00886) and by the University of Texas at Austin.

**Supplementary Material Available:** Tables of anisotropic thermal parameters and hydrogen atom parameters (8 pages). Ordering information is given on any current masthead page.

(25) Isci, H.; Dag, O.; Mason, W. R. *Inorg. Chem.* **1993**, *32*, 3909.

(26) Matsen, F. A. In *Technique of Organic Chemistry*, Vol. IX, *Chemical Applications of Spectroscopy*; West, W., Ed., Interscience Publication: New York, 1956.